Industrial Crops & Products 224 (2025) 120320

Contents lists available at ScienceDirect

Industrial Crops & Products

journal homepage: www.elsevier.com/locate/indcrop

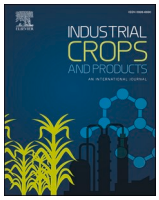

The soft template-assisted foaming technique's impact on biopitch-based porous carbon foam features

Adife Şeyda Yargıç *, Gamze Gündüz Meriç, Nurgül Özbay

Chemical Engineering Department, Engineering Faculty, Gulumbe Campus, Bilecik Seyh Edebali University, Bilecik 11100, Turkey

ARTICLE INFO

Keywords:
Biopitch
Carbon foam
Chemical activation
Hornbeam sawdust
Soft template P-123

ABSTRACT

Thermoplastic features, high carbon content, low ash level, and abundant phenolic chemical content of biopitch have made it a suitable precursor for carbonaceous materials. The present study aimed to investigate the utilization of a previously untested soft template-assisted foaming technique in the fabrication of biopitch-based carbon foam that provided brightness to the research in the literature. The hornbeam sawdust pitch-based carbon foams were formed by incorporating the non-ionic surfactant P123 into the synthesis solution. The research focused on understanding the effects of the foaming technique (conventional or template-assisted), template ratio, and chemical activation on the foam's physical, chemical, and mechanical properties via several analytical and characterization test methods. Raman spectroscopy, scanning and transmission electron microscopy analyses were performed to characterize the pore structures and carbon hybridization types, deducing highly aligned graphitic-like structures. Moreover, the mechanical strength of carbon foam was also enhanced via soft-template addition before foaming and diminished after chemical activation. The highest mechanical strength of 9.79 MPa with suitable thermal conductivity of 0.044 W/m.K and the lowest porosity of 71.41 % were attained when the template amount was 1 wt%. Surface areas of activated carbon foams ranged from 92.3 to 1121.2 m^2/g. Accordingly, the adjustable pore structures of the developed materials allowed them to be considered promising adsorbents according to the need to remove pollutants of different sizes. The results obtained from the study will provide valuable insights into the effectiveness of the soft template-assisted foaming technique in high-quality and hierarchically arranged graphitic carbon foam production and its potential applications in thermal insulation.

1. Introduction

Carbon-based materials are commonly used in a variety of fields because of their excellent electrical and thermal capabilities, unique lightweight nature, and resistance to corrosion (Deng et al., 2010; Wang et al., 2020; Wu et al., 2020; Xu et al., 2019; Yousefi et al., 2014; Zhang et al., 2017). These benefits make carbon foam an effective choice for many applications, including catalyst supports, filters, electrode materials, and heat protection (Chen et al., 2013; Kang et al., 2011; Zhang et al., 2015). Research on the usage of carbon foams (*CFs*) in thermal applications is widely ongoing because of their excellent comprehensive performance, and *CFs* are now one of the commercially available thermal insulation materials. A direct carbonization procedure can be used to produce carbon foam from polymers such as resin, polyurethane, sucrose, and melamine. It can also be obtained from mesophase pitch, where products perform better in terms of thermal insulation and mechanical strength (Sihn et al., 2012); however, to satisfy the needs of many modern uses, its thermal insulation performance still has to be improved.

Herein, the synthesis of foam-like bio-carbon derived from hornbeam sawdust biopitch, which could be used as a sustainable pitch substitute instead of fossil fuel, was reported. During wood production, sawdust waste usually spreads from trees and is traditionally disposed of via central burning. On the other hand, burning biomass would not only make the atmosphere less visible, but it would also affect the environment and release a lot of carbon dioxide, which would be harmful to human health (Zou et al., 2020). As people's comprehension of energy saving and environmental preservation has grown, sawdust waste has been completely used and transformed into a variety of goods that improve people's quality of life and productivity. For example, sawdust waste can be fermented to make mattresses or soilless flower culture substances; it is also a fuel source for the production of electricity (Imai

* Corresponding author.
E-mail addresses: seyda.guler@bilecik.edu.tr, aseydaguler@gmail.com (A.Ş. Yargıç).

https://doi.org/10.1016/j.indcrop.2024.120320
Received 24 June 2024; Received in revised form 6 December 2024; Accepted 11 December 2024
Available online 17 December 2024

et al., 2018) and used as a feedstock for building insulation components (Corinaldesi et al., 2016). Sawdust was utilized as the basic raw material for producing a novel biopitch-based insulating material in this investigation, thereby recycling waste resources.

In this study, the base process for the bio-based carbon foam generation was the foaming of hornbeam sawdust biopitch using the soft template-assisted method in a high-temperature/pressure reactor and chemical activation. The first-generation carbon foams produced by the thermal decomposition of thermoset phenolic foams had a homogeneous network structure but exhibited limited mechanical strength. The use of fossil fuel-based precursors such as coal, coal-tar pitch, and petroleum pitch with high carbon content has come to the forefront of studies on carbon foam production to overcome this disadvantage. Working with the mentioned precursors has significant limitations in terms of both environmental and cost, considering the required pretreatments and the applied rigid operating conditions (Yargıç et al., 2021b). The drawbacks noted above can be minimized by utilizing waste biomass-based precursors in carbon foam formation to assess renewable resources. Biomass tar is an acceptable precursor for carbonaceous material manufacturing due to its high carbon content, low ash level, and thermoplastic characteristics (Li et al., 2019; Yargic, 2021; Yargic and Ozbay, 2019). The investigation of foaming methods such as self-bubbling foaming (Fawcett and Shetty, 2010), template foaming (Mochida et al., 2000), and supercritical foaming (Li et al., 2009) in the manufacturing of carbon foam has been the focus of scientific inquiry in recent years. Soft templates such as F127, P123, and other block copolymers are utilized to produce porous carbons because of their controllable ordered mesopores, easy synthesis procedure, and preventable template removal strategies, as opposed to recently developed templates and self-templates (Wang et al., 2022). Asymmetric flask-like hollow carbonaceous structures (Chen et al., 2017), nitrogen-doped hierarchical porous carbon nanospheres (Xiong et al., 2017), and a hierarchical porous N, O, S-enriched carbon foam (Peng et al., 2019) are some of the porous carbon materials produced by involving soft templates. The approach employed in the study, which was of significant originality, entailed the combination of biopitch with a soft template before the foaming stage. This technique served as a standout method in the research and offered a novel approach to the subject matter. The production of bio-based carbon foam using the soft template method and its use in thermal insulation was illustrated for the first time based on our knowledge. Through a template technique, a non-ionic surfactant of triblock copolymer (Pluronic P123) was used to control porous structure with a regular morphology. The present paper was organized systematically to provide a clear presentation of the research findings. The layout followed a logical sequence of steps encompassing raw material characterization, pyrolysis, tar and biopitch characterization, foaming of biopitch via conventional and soft template-assisted methods, chemical activation, and carbon foam characterization.

2. Materials and Methods

2.1. Preparation of precursor for the foaming process

Through pyrolysis of hornbeam tree waste sawdust (*HS*, Eskişekir, Turkey), which contained 85.21 wt% volatile matter (ASTM E 872–82) and a high amount of lignin (30.92 wt%, ASTM D 1106–96) owing to preliminary and structural analyses, respectively, tar rich in phenolic compounds was generated. The vacuum distillation process was then applied to obtain biopitch-the precursor of carbon foam. A comprehensive evaluation was conducted on all of the biomass precursor, tar, and biopitch analyses in our previous searches (Yargıç et al., 2021a, 2021b). The slow pyrolysis method produced tar ($HS_{@400\ ^\circ C}$) with a 59.94 % C content and a 19.95 % yield when it was conducted at 400 °C under static conditions with a heating rate of 10 °C/min (Ozbay and Yargic, 2019; Yargic and Ozbay, 2019; Yargıç et al., 2021a). Elemental carbon content (73.93 %, Leco CNH628 S628), softening point (SP = 125.2 °C, Mettler Toledo FP90–83 HT), and acetone-insoluble fraction (*AI%* = 32.3 %) of biopitch, which was the heavy fraction of tar (Distillation conditions: T = 250 °C, P_{vacuum} = 50 mbar, t = 24 h, yield = 17.02 %) were calculated. In contrast to toluene- and quinolone-insoluble fractions (*TI* and *QI*), which were used to determine the solubility of fossil pitches, acetone was employed as the solvent for wood tar pitch analysis (Prauchner et al., 2001a). FT-IR analysis (Perkin Elmer Spectrum 100) revealed the presence of functional groups (e.g., -OH, C-H, C–O, C═O, C═C, –COOH) in the structures of all biomass, tar, and biopitch, including aliphatic, olefinic, aromatic, and phenolic chemicals that were unique to lignocellulosic-based materials. Evidence of the existence of phenolic compounds in the structure of wood-based tar was reported according to the ^{1}H NMR spectrum (Varian Mercury 300 MHz, 20.10 % of phenols and unconjugated olefins, 16.45 % of aromatic and conjugated olefinic compounds) (Ozbay and Yargic, 2019; Prauchner et al., 2001b). The biopitch's O content of 18.30 %, as determined by the elemental analysis, was identified to be corroborated by the presence of hydroxyl and carboxyl groups in the FT-IR spectrum. The biopitch underwent decomposition reactions between 200 °C and 620 °C, and it degraded by 56 % at 450 °C, as per the temperature profile that examined the biopitch's behavior against the thermal effect it will be exposed to in the high-pressure/temperature reactor.

2.2. Preparation and characterization of HS biopitch-based carbon foams

2.2.1. Green foam preparation without template

Hornbeam sawdust biopitch was foamed in a Parr reactor (4575B, Parr Instrument Company, USA) to create as-synthesized green foam. Nitrogen was added to the reactor to reach the beginning pressurized level of 1 MPa. The reactor temperature was subsequently increased to 450 °C at a rate of 2.5 °C/min, and the reactor was then allowed to stay at this temperature for 1 h. Finally, the reactor pressure was lowered to atmospheric pressure and allowed to reduce to an ambient temperature to generate the green pitch foams. As the pitch warmed up, the volatiles originated from the lightweight fractions as well as thermally degraded components functioned as "bubble agents" and promoted the foaming material's volume. As a result of the shear tension generated through the bubbles expanding under pressure, the pitch particles were arranged perpendicular to the exterior of the bubbles. The biopitch hardened when the temperature got higher, and the foam matrix was fixed (Tsyntsarski et al., 2010). According to Beechem et al. (2005), the pitch removed volatiles as cells enlarged due to a decrease in pressure-induced stress. The yield achieved by generating carbon foam from hornbeam sawdust biopitch was estimated to be approximately 41.56 %.

2.2.2. Green foam preparation with soft template P123

The process involved mixing a specific amount of P123 and biopitch by the template ratio to be used, foaming at 450 °C in the high temperature/pressure reactor to produce foam via a soft template. Various scientific research examining thermograms related to the thermogravimetric analysis of Pluronic P123 revealed that the surfactant was fully degraded at 400 °C, following a rapid weight loss after 200 °C (Gonçalves et al., 2018; Pham et al., 2019; Zakaria et al., 2013). No additional procedure was required to remove the template since P123 in the as-synthesized green foam structure may be entirely broken down by heat treatment at temperatures much lower than 1050 °C, which was the carbonization temperature (Zhao et al., 2015).

2.2.3. Chemical activation and carbonization processes

Numerous attempts have been made to use different physical and chemical activation processes to create and modify the microstructures of porous carbonaceous materials. Considering the research about the chemical activation process conducted to date (Sun and Webley, 2011; Wang and Kaskel, 2012; Yargic and Ozbay, 2019), the mechanisms of solid-solid phase reactions initially formed between potassium hydroxide (KOH) and carbon in the foam matrix, and then continuing

solid-liquid phase reactions were presented in detail below: *i)* chemical activation (Eqs. (1), (4), and (6)); *ii)* physical activation (Eqs. (2), (3), (5), (7–9)); and *iii)* as-formed metallic potassium (Eqs. (1), (4), and (6)) integration to the carbon matrix during the activation and the carbon lattice's expansion.

$$6KOH + 2C \rightarrow 2K + 3H_2 + 2K_2CO_3 \quad (1)$$

$$2KOH \rightarrow K_2O + H_2O \quad (2)$$

$$K_2CO_3 \rightarrow K_2O + CO_2 \quad (3)$$

$$K_2CO_3 + 2C \leftrightarrow 2K + 3CO \quad (4)$$

$$K_2O + H_2 \rightarrow 2K + H_2O \quad (5)$$

$$K_2O + C \rightarrow 2K + CO \quad (6)$$

$$C + H_2O \rightarrow CO + H_2 \quad (7)$$

$$CO + H_2O \rightarrow CO_2 + H_2 \quad (8)$$

$$CO_2 + C \rightarrow 2CO \quad (9)$$

Mainly, the chemical activation of several forms of carbon with KOH as the activating agent reflected great promise due to the lower activation temperature of the process, as well as obtaining the final products with higher yields, ultrahigh specific surface area, and certain micropore size distributions (Wang and Kaskel, 2012). The chemical activation process integrating potassium hydroxide (Tondi et al., 2010) at a foam: KOH ratio of 1:1 (w/w) was used to enhance the surface areas and porous structures of the as-synthesized green foams formed by both the traditional foaming and template-assisted methods. The as-synthesized green foam and activated foams were subjected to heat treatment at a rate of 5 °C/min under a nitrogen environment (100 mL/min) up to 1050 °C and held for 2 h at the final temperature as part of the carbonization step. Following the elimination of K^+ ions from the structure by washing the activated materials with distilled water until the pH value was near neutral, the samples were dried in an oven at 110

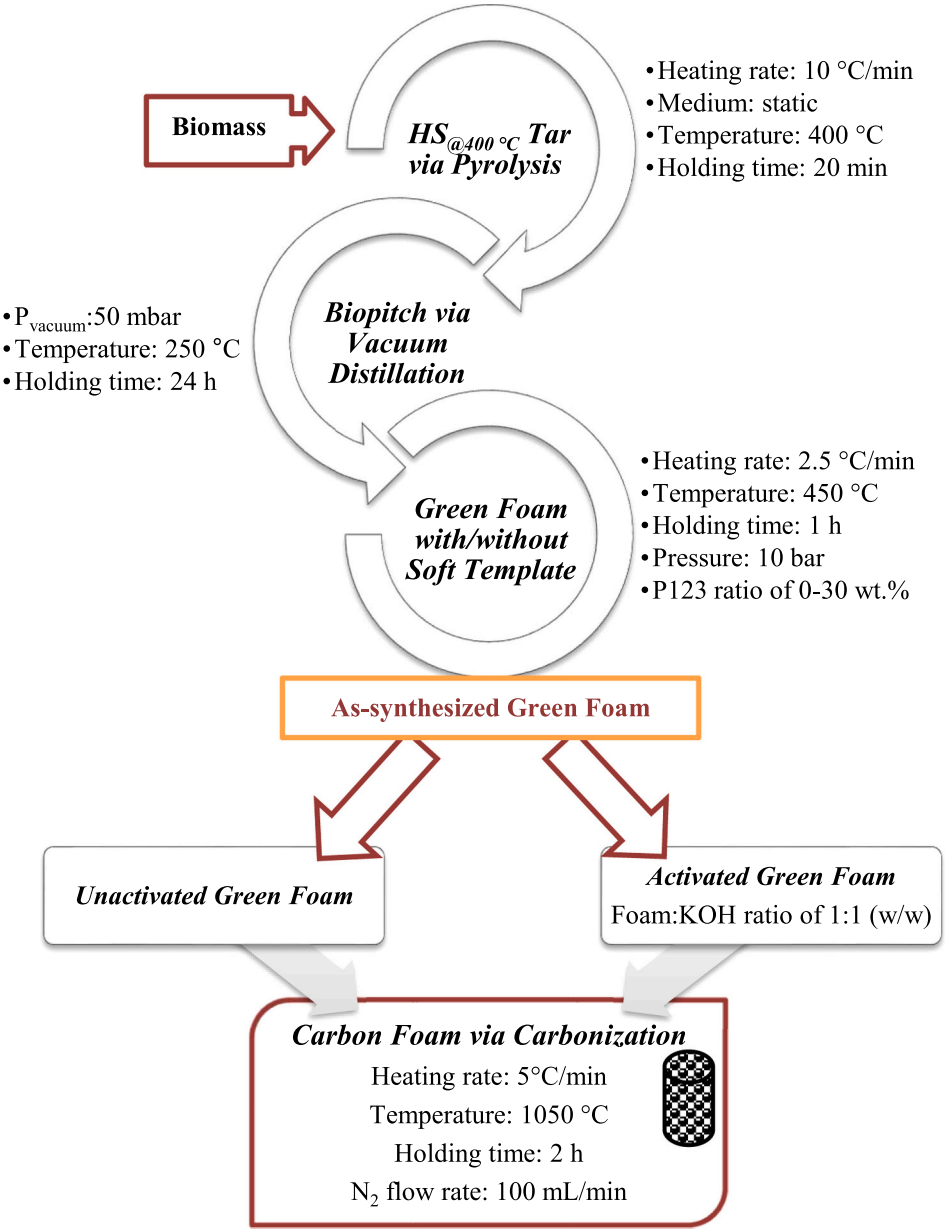

Fig. 1. The schematic diagram of carbon foam production via the soft template-assisted foaming method.

°C, thus the generation of activated carbon foam was achieved. The nitrogen gas supplied into the system helped to eliminate the volatile compounds and kept the foam from smashing at elevated temperatures through the carbonization step. Carbon foams formed from hornbeam sawdust-based biopitch without the contribution of a template were coded as unactivated (*HSPCF*) and chemically activated (*HSPACF*) according to the activation state. The carbon foams produced with a soft template were assigned the code *HSP-P−x* or *HSPA-P−x* by considering the activation process. The P123 template ratio contributed by 1, 5, 10, 20, and 30 wt% was denoted by the character "*x*" in the current case. The soft template-assisted method of producing carbon foam from biomass was displayed schematically in Fig. 1.

2.2.4. Characterization of carbon foams

To further understand the properties of the foams, elemental analysis (Leco CNH628 S628), which measures the CHN content, was implemented in the first step. The elemental compositions of *CFs* were determined by CHN analysis, and O contents were calculated by difference. Based on the measurement employing Micromeritics ASAP 2020 volumetric adsorption apparatus, the textural properties (surface area (S_{BET}) and pore volume (V_{total})) of biopitch-based *CFs* were determined through the Brunauer-Emmett-Teller (BET) method following a 6-hour degassing at 300 °C under vacuum. The Density Functional Theory (DFT) was followed to analyze the pore size distributions, micropore volume (V_{micro}), and mesopore volume (V_{meso}) of foams developed without employing the template strategy. A helium gas pycnometer (Micromeritics, Accupyc II 1340) was employed to measure the true densities after the bulk densities were calculated by weighing foams with particular sizes. The theoretical and actual volumes of the foams were represented by the symbols V_t and V_a in Eq. (10), and the porosity (%) values were calculated using Eq. (10) (Ning et al., 2017).

$$Porosity(\%) = (V_t - \quad V_a)/V_t \tag{10}$$

The crystal structures and the d-spacing values were assessed using a Panalytical Empyrean x-ray diffraction apparatus (2θ = 0°-80°) with CuKα radiation (λ = 0.15406 nm). Transmission and scanning electron microscopes were used to characterize the carbon foams' microstructure and surface morphology. The foams' surface morphologies were recognized by scanning electron microscopy (Zeiss Supra VP 40) images obtained with platinum sputter-coated (Quorum Q 150 R ES DC Sputter) materials. In addition, confocal Raman spectra were recorded by the Renishaw Raman inVia microscope, and compressive strength measures at a 0.5 mm/min loading rate were performed by a Shimadzu AG-IC 100KN tensile/compression equipment. The thermal conductivity measurements (C-Therm TCI 2 A) were carried out at room temperature, and a transmission electron microscope (TEM, JEOL 1220 JEM, 80 keV) was employed to evaluate the textural characteristics of the foams generated under ideal experimental conditions determined through the compressive strength, surface area, and crystal structure.

3. Results and Discussion

3.1. Elemental Analysis

Table 1 demonstrated the variations in H/C and O/C ratios with C-H-N (%) elemental analysis values of the *HS*-based foams, concerning both template fraction and chemical activation step. The carbon content of the foams ranged from 86.6 % to 55.5 %, which was significantly greater than the C content of feedstock (45.99 % C) and tar (59.94 % C). The carbon foam produced without the implementation of a template approach had 86.63 % C, and the C content lowered to 82.27 % following the chemical activation stage. When the template was not used, the *CFs*' C amount had higher percentages than that of biopitch, and the O amounts' were lower, based on the fact that biopitch's C and O contents were 73.33 % and 18.30 %, respectively. The special cylindrical molds were filled with a blend of P123 ($EO_{20}PO_{70}EO_{20}$) and biopitch and placed in the reactor, the non-ionic copolymer led to foaming when the template approach was applied. Implementing a soft-template method raised the proportion of oxygenated groups added to the synthesis mixture as the template ratio increased from 1 % to 30 % by weight. Since oxygenated entities promoted self-combustion throughout the heating process applied in the foaming and carbonization steps, the elemental C contents in the c-foam structures were reduced. Moreover, with chemical activation under an alkaline medium, the carbon in the foam reacted with potassium hydroxide, reducing the C ratio in the activated c-foam structure. The O/C ratio of c-foam created without a template was 0.09, while the ratio of c-foam that included the P123 additive ranged from 0.14 to 0.49. The soft template-assisted activated c-foams were found to have O/C ratios varying from 0.26 to 0.59. In the current case, activated c-foams with higher O and lower C contents than non-activated c-foams were produced by applying the activation following the foaming process.

Table 1
Elemental analysis of *CFs* produced at 1 MPa and 450 °C.

Foam code	C (%)	H (%)	O (%)	N (%)	HHV (MJ/kg)	H/C	O/C
Produced by conventional method without a template							
HSPCF	86.63	0.59	10.81	1.97	28.20	0.08	0.09
HSPACF	82.27	0.82	15.46	1.45	26.21	0.12	0.14
Produced by a soft template-assisted method							
HSP-P−1	83.05	1.01	15.22	0.73	26.79	0.15	0.14
HSP-P−5	82.44	1.04	15.86	0.67	26.52	0.15	0.14
HSP-P−10	79.01	0.94	19.72	0.33	24.53	0.14	0.19
HSP-P−20	63.94	0.83	34.92	0.31	16.53	0.16	0.41
HSP-P−30	60.01	0.54	38.89	0.56	14.06	0.11	0.49
HSPA-P−1	72.56	1.16	25.47	0.81	21.62	0.19	0.26
HSPA-P−5	68.08	0.58	30.91	0.43	18.29	0.10	0.34
HSPA-P−10	66.95	1.01	31.57	0.47	18.41	0.18	0.35
HSPA-P−20	62.88	0.75	35.96	0.41	15.87	0.14	0.43
HSPA-P−30	55.49	0.37	43.78	0.37	11.40	0.08	0.59

3.2. XRD Analysis

The crystalline structures of the hornbeam biopitch-based carbon foams were analyzed through XRD, as shown in Fig. 2. Between 2θ = 10° and 30°, a wide band of the stacked graphitic basal plane (0 0 2) related to carbonaceous materials was observed. The peak of this band was found to be alongside 2θ = 23° (Apaydın-Varol and Erülken, 2015; Girgis et al., 2002; Lopez et al., 2013; Tushar et al., 2012; Yargic and Ozbay, 2019; Zhang et al., 2014). This band was indicative of the presence of graphitic structures in the samples. Graphitic carbon materials, such as graphene and graphite, have unique mechanical, electrical, and thermal properties, and are widely used in various applications, including electronics, energy storage, and catalysis. Therefore, the presence of this band is of great interest and significance in the study of carbon-based materials. At high temperatures, typically ranging between 1400 and 1500 °C, a characteristic (0 0 2) peak is observed in substances like eucalyptus lignin and reinforced phenol-formaldehyde resin-based fibers that share an identical structure. The development of this peak at a mild temperature of 1050 °C during carbonization was supposed to be associated with the thermoplastic properties of biopitch and the existence of low-molar weight species (Yargıç, 2017). The present disclosure pertained to the 2D configuration of carbon layers in graphite-like materials. Specifically, it was ascertained that this configuration featured planes of (1 0 0) and (1 0 1) at angles between 2θ = 41 and 45° (Prauchner et al., 2005; Wang et al., 2008). The result denoted that the process of condensation of aromatic rings into two-dimensional clusters commenced at an operational temperature of 1050°C. This finding is of relevance to the study of the properties and behavior of aromatic organic compounds, particularly in high

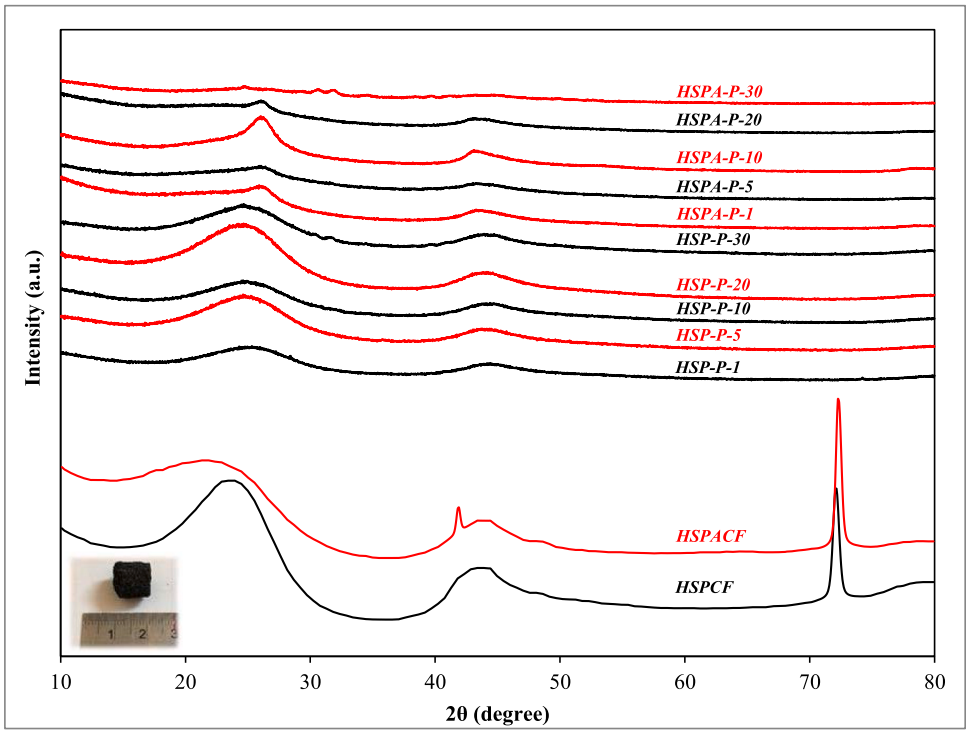

Fig. 2. XRD patterns of carbon/activated foams produced by conventional foaming method and template-assisted method.

temperature and pressure conditions, and may have practical applications in fields such as materials science and industrial chemistry. Table 2 informed that the d_{002} spacing values close to $2\theta = 25^{\circ}$ differed from 0.3409 to 0.4162 nm. The d-spacing results revealed the non-graphitized carbon structure and were higher than the value of 0.3350 nm ascribed to graphite (Yargic et al., 2023). The assistance of a soft template for foaming shifted the peak to higher angles and resulted in reduced d_{002} spacing, indicating an improved level of graphitization. Moreover, the chemical activation of template-assisted foams resulted in more regular structures.

The diffraction peaks observed near $2\theta = 23^{\circ}$ and 43° were attributed to the hexagonal carbon (0 0 2) and hexagonal graphite (1 0 0) planes of partially graphitized structures, respectively (Fayos, 1999; Hull, 1926; Li et al., 2015; Lipson and Stokes, 1942; Strano et al., 2002; Wang and Kaskel, 2012). Moreover, the diffraction peak observed at $2\theta = 72^{\circ}$ was indicative of the presence of orthorhombic graphite (Luo et al., 2013). The present study has revealed that the chemical activation of carbon foams, despite exhibiting similar diffraction patterns, caused a reduction in the intensity of reflections of the (0 0 2) and (1 0 0) planes. These findings suggest that chemical activation can significantly impact the structural properties of carbon foams and, therefore, should be considered when designing and characterizing such materials. The addition of 1 wt% P123 template during the preparation of foams was observed to significantly enhance the reflection intensity of (0 0 2) and (1 0 0) planes in the x-ray diffraction patterns. This noticeable increase in reflection intensity pointed towards the development of a more crystalline structure for the aforementioned foams. The reflection intensities of particular planes in the foam with *HSPA-P−30* code showed the most inferior peaks among all patterns. This result indicated that *HSPA-P−30* may comprise lower crystallinity or exhibit more amorphous characteristics than the other foams. The investigation of carbon foam's crystallographic properties unveiled valuable insights that could steer further research to explore its diverse industrial applications. These findings can be leveraged to enhance the application of carbon foam in various sectors.

Table 2
XRD parameters of carbon foams.

CF code	2θ (002) (°)	d_{002} (nm)	ACF code	2θ (002) (°)	d_{002} (nm)
HSPCF	23.43	0.3794	***HSPACF***	21.33	0.4162
HSP-P−1	25.32	0.3515	***HSPA-P−1***	26.12	0.3409
HSP-P−5	24.61	0.3614	***HSPA-P−5***	26.05	0.3418
HSP-P−10	24.61	0.3614	***HSPA-P−10***	26.03	0.3420
HSP-P−20	24.65	0.3609	***HSPA-P−20***	26.08	0.3414
HSP-P−30	24.66	0.3607	***HSPA-P−30***	25.91	0.3436

3.3. Textural Analysis

A unique pore structure found in carbon foam is characterized by an open cell structure, wherein the majority of macropores (cells) are interconnected, in contrast to the other morphologies of carbon materials, which include fibrous, tubular, spherical, platelet, and granular structures (Inagaki et al., 2015). Carbon foam durability is significantly affected by the micropore and mesopore morphology (Chen et al., 2006). Applying nitrogen-sorption analysis and the DFT method, the pore volume, surface area, and pore size of carbon foams formed in the conventional bubbling method were ascertained. The results were listed in Table 3, and Fig. 3 provided the nitrogen adsorption/desorption isotherms and pore size distribution graphs. The isotherm type indicated the presence of micropores in carbon foams based on the increase in adsorbed volume at a relative pressure of $P/P_0 < 0.1$. Further evidence for the formation of macropores was provided by the rise in adsorbed

Table 3
Textural properties of *CFs* prepared without using templates.

Foam code	S_{BET} (m^2/g)	V_{total} (cm^3/g)	V_{micro} (cm^3/g)	V_{meso} (cm^3/g)	D_{av} (nm)
HSPCF	59.8	0.037	0.018	0.019	1.22
HSPACF	1004.2	0.423	0.392	0.031	1.22

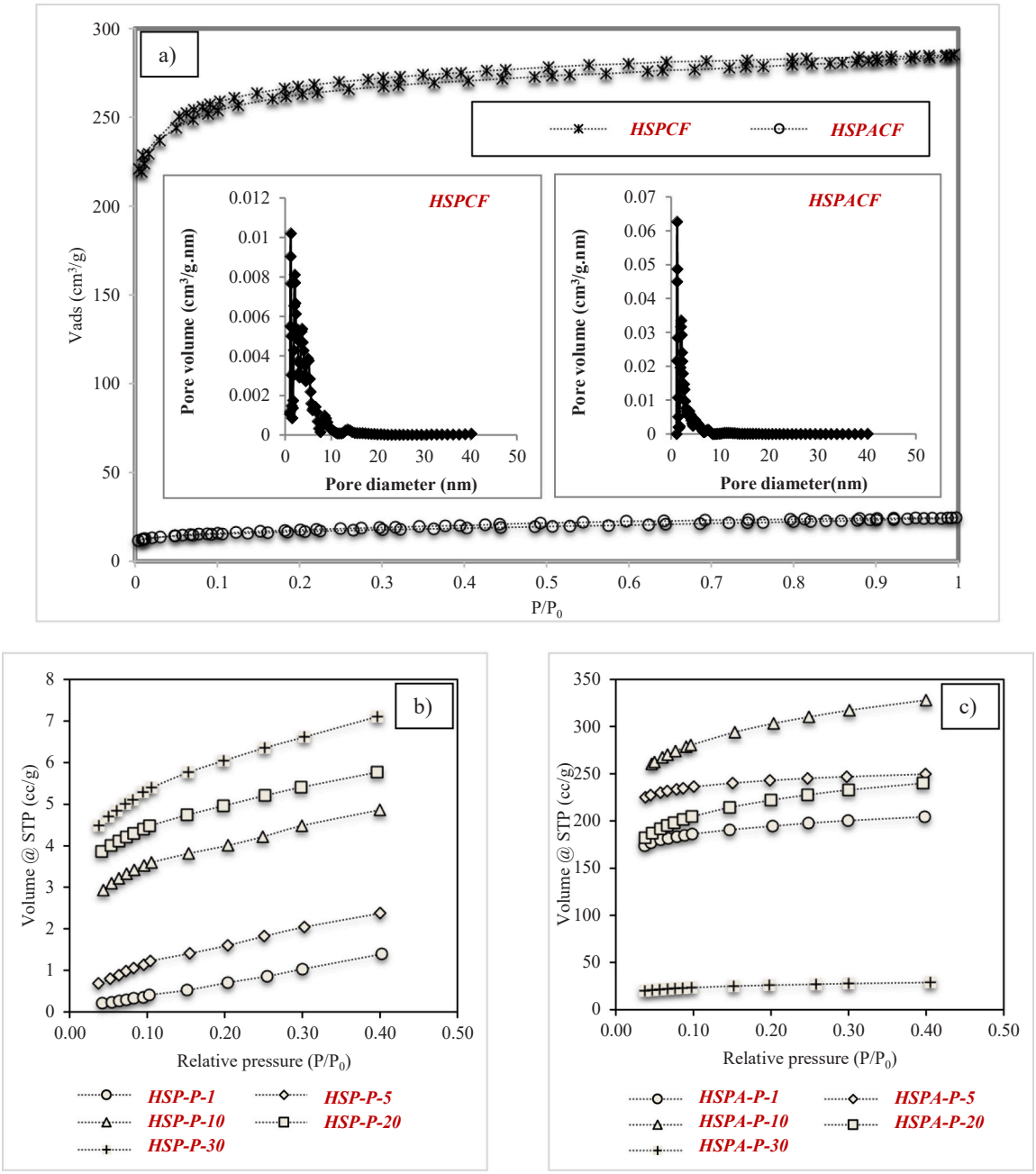

Fig. 3. (a) Nitrogen adsorption/desorption isotherms and DFT pore size distribution graphs for carbon foams produced without using templates, (b) and (c) adsorption isotherms ($0<P/P_0<0.4$) of carbon foams produced via template-assisted method.

volume following the relative pressure of $P/P_0> 0.9$, and the typical distribution of mesopores in the foams was shown by the tendency to rise in P/P_0 range of 0.01 and 0.30. The carbon foams' nonuniform-porous structures were commonly explained by the hysteresis that emerged in the adsorption and desorption isotherms (Yargic et al., 2023). *HSPCF* carbon foam's surface area, which was previously smaller at 59.8 m^2/g, improved to 1004.2 m^2/g for *HSPACF* because of the formation of tiny pores and cracks in the framework following chemical activation, confirmed by SEM analysis. The rise in pore volume, from 0.037 cm^3/g for *HSPCF* to 0.423 cm^3/g for activated *HSPACF*, was consistent with the aforementioned condition. The IUPAC classification of meso and micropores was supported by type IV isotherm in the foams' nitrogen adsorption/desorption isotherms. It was noticed that *HSPCF* and *HSPACF* foams had the same mean pore diameters (D_{av}, nm) of 1.22 nm. The activated carbon foam's pore size distribution was identified to be more uniform than that of the non-activated carbon foam based on Fig. 3a.

Fig. 3b and c displayed the adsorption isotherms between 0.0 and 0.4 relative pressure range that were analyzed to determine the multi-point BET surface area of foams developed via the soft template-assisted method. Table 4 revealed that the multi-point S_{BET} value increased

Table 4
S_{BET} of carbon/activated foams prepared via template-assisted method.

CF code	S_{BET} (m^2/g)	ACF code	S_{BET} (m^2/g)
HSP-P–1	4.8	***HSPA-P–1***	735.9
HSP-P–5	7.0	***HSPA-P–5***	946.6
HSP-P–10	13.9	***HSPA-P–10***	1121.2
HSP-P–20	17.2	***HSPA-P–20***	808.1
HSP-P–30	21.1	***HSPA-P–30***	92.3

from 4.8 m^2/g to 21.1 m^2/g whenever the template ratio varied from 1 to 30 wt percent when soft template P123 was employed in the foaming process, and no chemical activation was applied. The soft template elimination by carbonization and the interconnected pores development in the carbon foam structure resulted in an apparent rise in surface area. Heat treatment was the sole method used to remove the template that was still present in the structure of the green foam when the foaming process was applied by adding P123 to the synthesis medium. In contrast to carbon foams with micropores, the carbonization of the green foam at 1050 °C caused the expansion of void sizes within the cells and, consequently, the reduction of surface area due to the cracks that were created in the foam framework because of the template degradation and the spontaneous combustion supported by oxygen species in P123. In a similar manner, incorporating a P123 template in the 1–10 wt% range resulted in a proportionate increase in the surface area of activated carbon foams. The surface areas of the activated carbon foams with 20 or 30 wt% P123 templates were found to diminish as a result of the shape deformations that the carbonization and activation processes caused in the structure. With a value of 1121.2 m^2/g, *HSPA-P−10* coded foam had the largest surface area among the P123 template-assisted activated foams. Following the chemical activation step, the surface area value of *HSP-P−10* coded carbon foam (13.9 m^2/g) was increased by approximately 81 times to produce *HSPA-P−10*. SEM images affirmed that the micropores in the *HSPA-P−10* activated foam's cell walls were the probable cause of this change in surface area. A great number of tiny pores were created inside the macropores of carbon materials as a side effect of the interaction between the carbon foam and the activating agent. The fact that the micropores were subsequently etched by KOH to form comparatively large mesopores explained the loss in surface area for foams prepared by incorporating more than 10 wt% of the soft template (Xiong et al., 2012).

3.4. Electron Microscopic Analyses

The morphological structures of non-activated and activated carbon foams created through biopitch foaming using conventional and soft template-assisted techniques were revealed by the SEM images shown in Figs. 4 and 5. The porous structures of the *HSPCF* and *HSPACF* foams were apparent at 100x magnification through the SEM images in Fig. 4. It was revealed that the activation of *HSPCF* with KOH led to microcracks in the structure alongside fractures in the cell walls and strut joints of the resulting *HSPACF* foam. Although the surface area was increased, the compressive strength was decreased due to this structural change. The structures of carbonized and activated foams formed through conventional foaming were found to have cells of different sizes within 50–400 μm.

SEM images of foams generated utilizing P123 as a soft template were displayed in Fig. 5. The chemical activation of soft template-assisted carbon foams resulted in structural cracks that resembled the morphology of activated foam produced by the conventional foaming technique. The carbon foam (*HSP-P−1*) formed when 1 % by weight of P123 was utilized as the template shown in Fig. 5a contained cells ranging in size from 200 to 800 μm and voids ranging from 110 to 460 μm. Fig. 5b demonstrated that the cell sizes of the activated foam (*HSPA-P−1*) varied between 400 and 700 μm, and the size of the voids changed between 150 and 400 μm. The carbon foam (*HSP-P−5*) formed by increasing the P123 template ratio from 1 % to 5 % by weight displayed a more homogeneous cell size distribution between 300 and 920 μm. Meanwhile, the void sizes of *HSP-P−5* (30–390 μm) altered between 90 and 570 μm as a result of chemical activation (*HSPA-P−5*) (Fig. 5c and d). The carbon foam (*HSP-P−10*) with higher cell sizes (310−975) was produced upon increasing the P123 ratio from 1 % to 10 % by weight (Fig. 5e). On the other hand, the porosity of the activated foam *HSPA-P−10* increased via the activation process, and sizes of cells and voids varied in the ranges of 270–845 μm and 255–625 μm, respectively (Fig. 5f). When the soft template ratio was increased to 20 % by weight, as shown in Fig. 5g and h, void sizes of *HSP-P−20* varied between 60 and 310 μm, while porous *HSPA-P−20* had a high rate of structural cracks. While the P123 ratio was 30 wt%, cell frameworks were not regularly formed in the *HSP-P−30* carbon foam, as well as inhomogeneous voids in the 45–510 μm size range appeared (Fig. 5i). Substantial microvoids were detected in the *HSPA-P−30* coded activated foam's structure as seen in Fig. 5j.

The TEM images (Fig. 6) evaluated for the clarification of the textural characteristics proved that the carbon foams had significant amorphous networks with pores and the noticeably graphitic carbon areas yielded due to the coincidence of graphene layers in all carbon foams. The shift to the right of the typical graphite peak (0 0 2) after the chemical activation step was likely due to a part of the biopitch's amorphous carbon converting into crystalline graphite, as indicated by the XRD patterns.

3.5. Physical, Thermal and Mechanical Properties

Specifically, Luo et al. (2013) stated that the density was considered to be the main factor influencing closed-cell foams' thermal conductivity and mechanical properties. The compressive strength measurements related to the densities and porosity degrees of the carbon foams were displayed in Table 5. As porosity and pore volume increased, compressive strength reduced, which was in line with previous reports (Luo et al., 2013; Yargic and Ozbay, 2019), such that the chemically activated foam *HSPACF* had a porosity that was 4.2 % greater relative to the *HSPCF*. Foams created using a soft template possessed higher bulk and true densities than *HSPCF* carbon foam. The bulk and true densities of hornbeam biopitch-based foams were in ranges of 0.13–0.50 g/cm^3 and 1.64–1.99 g/cm^3, respectively. The implementation of the chemical activation process resulted in an increase in true density and a reduction in bulk density, as well as a development in porosity. Upon analyzing the mechanical properties, it was determined that *HSPACF*-coded activated foam, which had a strength of 0.258 MPa, was created following the chemical activation procedure, whereas the compressive strength of *HSPCF* carbon foam was 1.681 MPa. The analysis revealed that the carbon and activated foams' respective compressive strengths ranged

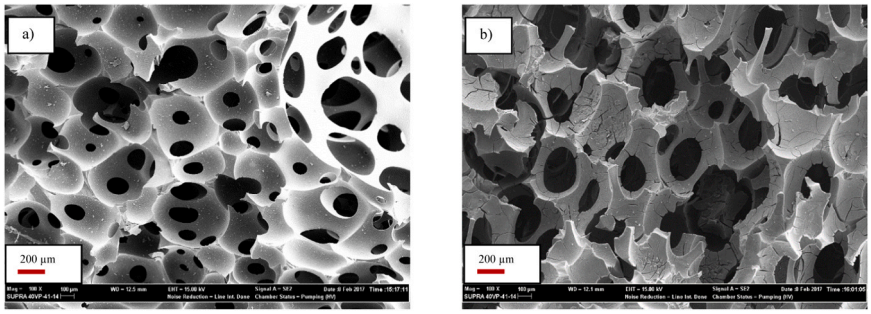

Fig. 4. SEM images of (a) *HSPCF* and (b) *HSPACF*.

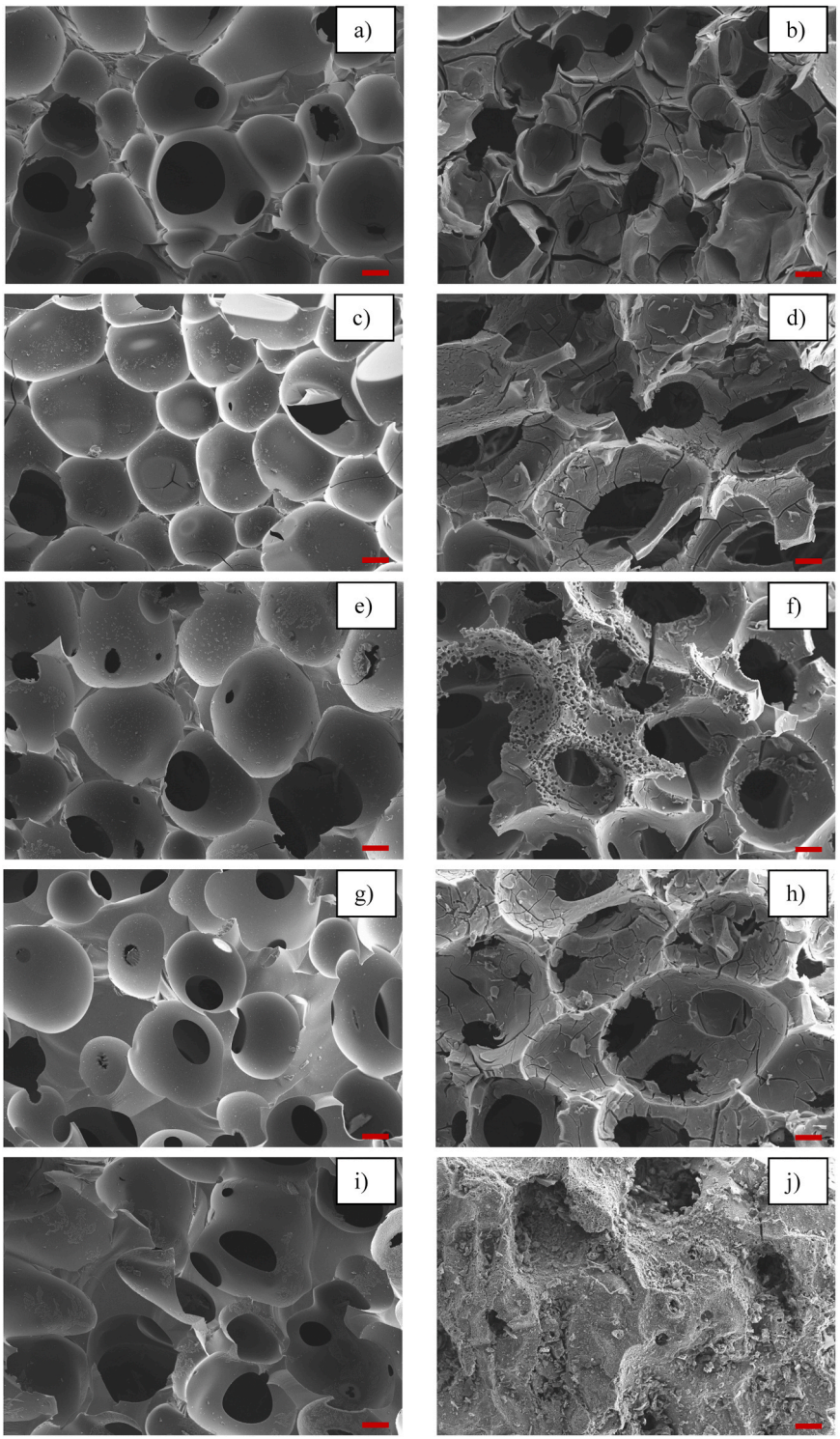

Fig. 5. SEM images (100x) of (a) *HSP-P-1*, (b) *HSPA-P-1*, (c) *HSP-P-5*, (d) *HSPA-P-5*, (e) *HSP-P-10*, (f) *HSPA-P-10*, (g) *HSP-P-20*, (h) *HSPA-P-20*, (i) *HSP-P-30,* and (j) *HSPA-P-30* (scale 200 μm).

from 1.681 to 9.793 MPa and 0.258–0.493 MPa, respectively. The chemical activation process led to an increase in porosity, which in turn caused the compressive strength of the foams to diminish, as evidenced by evaluations of surface area and morphology versus mechanical properties. Relative density (D^*/D_s) improvements were associated with either a decrease in cell edge length or an increase in cell wall thickness. Higher compressive strength was facilitated by a thicker cell wall and a shorter cell edge (Chen et al., 2006). The thermal conductivity of a material is significant concerning the intended use. The thermal conductivity of commercial carbon foams broadened to include ranging from 0.05 to 210 W/m.K (Gallego and Klett, 2003). Compared to graphite foams with thermal conductivities of 100–200 W/m.K, phenolic-based foams have thermal conductivities in the range of 0.06–0.24 W/m.K, and those of natural resource-based foams are lower than 0.2 W/m.K (Jana, et al., 2014; Lei et al., 2010; Mercuri et al., 1968; Nicholson and Thomas, 1973). The thermal conductivity coefficients of

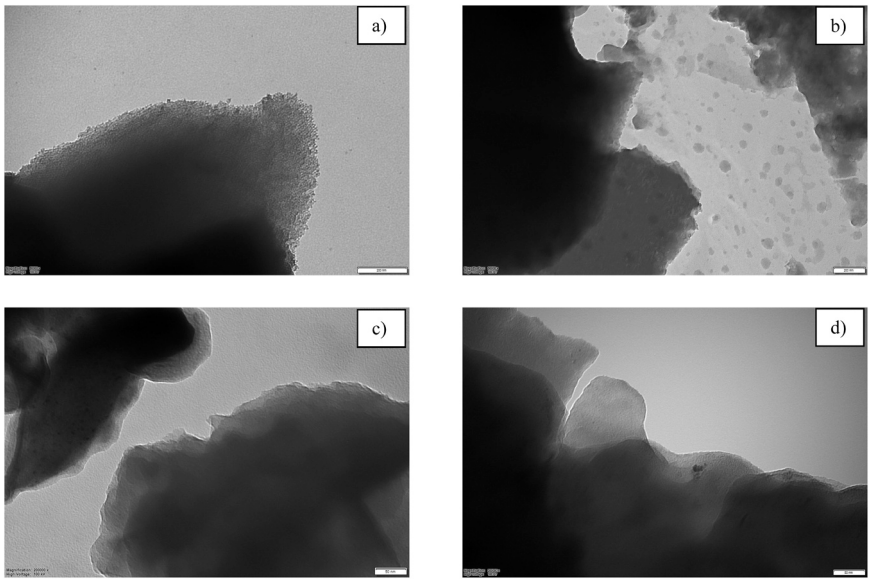

Fig. 6. TEM images of (a) *HSPCF*, (b) *HSPACF*, (c) *HSP-P-1*, and (d) *HSPA-P-1*.

Table 5
Carbon foams' compressive strength, density, and porosity (%).

Foam code	Compressive strength (MPa)	Bulk density (D*, g/cm^3)	True density (D$_s$, g/cm^3)	Porosity (%)
Produced without applying the template technique				
HSPCF	1.681	0.19	1.64	88.55
HSPACF	0.258	0.16	1.99	92.24
Produced using a soft template				
HSP-P−1	9.793	0.50	1.75	71.41
HSP-P−5	3.549	0.40	1.73	76.97
HSP-P−10	3.305	0.38	1.77	78.39
HSP-P−20	2.411	0.39	1.75	77.55
HSP-P−30	2.189	0.34	1.79	80.87
HSPA-P−1	0.493	0.21	1.73	88.08
HSPA-P−5	0.379	0.15	1.80	91.44
HSPA-P−10	0.374	0.13	1.82	92.74
HSPA-P−20	0.339	0.25	1.81	86.11
HSPA-P−30	0.278	0.41	1.73	76.29

the *HSPCF* and *HSP-P−1* labeled carbon foams developed within this study were 0.056 and 0.044 W/m.K., respectively. Thermal insulation components are specified by European standards as those with a thermal conductivity coefficient of less than 0.065 W/m.K. As a result, it became clear that the hornbeam biopitch-based carbon foams produced for this study might be classified as a form of thermal insulation material.

3.6. Raman Spectra Analysis

Raman spectroscopy analyses were carried out to detect the hybridized carbon bonds in the materials; thus, carbon foams' representative Raman spectra were displayed in Fig. 7. Characteristic peaks attributed to D-band (the formation of amorphous and graphite type carbon via sp^3 hybridization) and narrower graphite G-band (formation of carbon in sp^2 regular structures) types were detected at wavelengths of ~1343 cm^{-1} and ~1600 cm^{-1}, respectively (Kang and Lee, 2016).

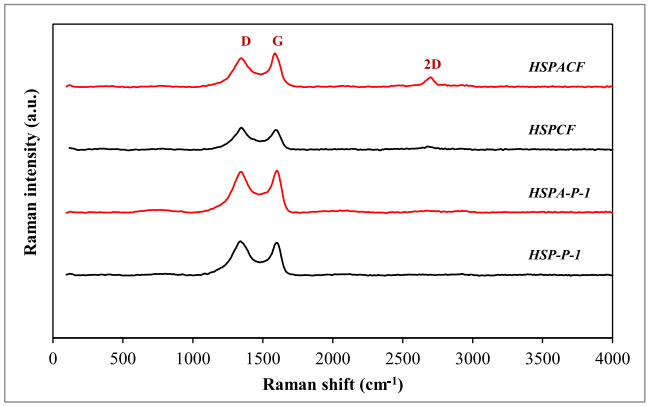

Fig. 7. Raman spectrums of carbon foams.

Typical Raman bands of carbonaceous materials, including graphene, are referred to as G and 2D bands. Temperature changes and chemical doping have a direct effect on these bands. Both the G and 2D bands' form, intensity, and position change with the graphene layers' number. The D-band provides information about the degree of defects and irregularities in the graphene's crystal structure, such as edge defects and heteroatom participation (Kılıç, 2019). The intensity of the 2D band at ~2700 cm^{-1} increases and appears as a sharper peak as the material gets closer to the monolayer graphene structure. However, the peak's intensity falls, and it does not give a smooth peak appearance when more than one peak overlaps as the layers' number increases. The presence of multiple layers with certain defects in foams other than *HSPACF* caused the 2D-band to broaden, as shown in Fig. 7. The lower D-band intensity in the Raman spectrum was associated with the higher degree of graphitization of carbon foams, whereas the strong D-band formation was indicative of the potential occurrence of partial lattice defects depending on the abundance of pores in a graphene monolayer (He et al., 2016; Li et al., 2011; Yargic and Ozbay, 2019).

4. Conclusions

Carbon foams' superior performance and adjustable 3D porous structure, broadly classified into two main groups of graphitic and vitreous, have attracted increasing attention from researchers. Coal tar- or

petroleum-based pitches are typically foamed, carbonized, and then graphitized to produce graphitic carbon foams with outstanding thermal stability. Investigations on ways to improve product abilities according to the application area and the utilization of sustainable precursors for the generation of carbonaceous materials, which are capable of several potentials among high-tech materials, have received a great deal of interest. This study was intended to evaluate the hornbeam sawdust biopitch as a precursor for the generation of carbon foam with adjustable properties. In this specific situation, the two unique strategies compared in the first step were foaming of biopitch or biopitch-soft template (P123) mixture. Besides, the significance of chemical activation under an alkaline medium and the soft-template technique on the features of carbon foams were thoroughly examined. The characterization results indicated that hornbeam sawdust biopitch could be used to produce graphitic carbon foams with sp^2 and sp^3 hybridized carbon atoms, highly porous structures, and a wide range of surface areas. The hierarchically ordered foams from waste biomass were projected to be beneficial as both adsorbent and thermal insulation materials because of these adaptable properties.

CRediT authorship contribution statement

Adife Seyda Yargic: Writing – review & editing, Visualization, Project administration, Investigation, Formal analysis, Conceptualization. **Nurgül Özbay:** Supervision. **Gamze Gündüz Meriç:** Writing – original draft, Visualization, Investigation, Formal analysis.

Declaration of Competing Interest

The authors declare the following financial interests/personal relationships which may be considered as potential competing interests: Adife Seyda YARGIC reports financial support was provided by TUBITAK. If there are other authors, they declare that they have no known competing financial interests or personal relationships that could have appeared to influence the work reported in this paper.

Acknowledgements

The authors would like to thank The Scientific and Technological Research Council of Türkiye (TÜBİTAK) under the Grant Number 219M104 for financial support.

Data availability

No data was used for the research described in the article.

References

Apaydın-Varol, E., Erülken, Y., 2015. A study on the porosity development for biomass based carbonaceous materials. J. Taiwan Inst. Chem. Eng. 54, 37–44. https://doi.org/10.1016/j.jtice.2015.03.003.

Beechem, T., Lafdi, K., Elgafy, A., 2005. Bubble Growth Mechanism In Carbon Foams. Carbon 43 (5), 1055–1064. https://doi.org/10.1016/j.carbon.2004.11.046.

Chen, S., He, G., Hu, H., Jin, S., Zhou, Y., He, Y., He, S., Zhao, F., Hou, H., 2013. Elastic carbon foam via direct carbonization of polymer foam for flexible electrodes and organic chemical absorption. Energy Environ. Sci. 6 (8), 2435–2439. https://doi.org/10.1039/C3EE41436A.

Chen, C., Kennel, E.B., Stiller, A.H., Stansberry, P.G., Zondlo, J.W., 2006. Carbon foam derived from various precursors. Carbon 44 (8), 1535–1543. https://doi.org/10.1016/j.carbon.2005.12.021.

Chen, C., Wang, H., Han, C., Deng, J., Wang, J., Li, M., Tang, M., Jin, J., Wang, Y., 2017. Asymmetric flasklike hollow carbonaceous nanoparticles fabricated by the synergistic interaction between soft template and biomass. J. Am. Chem. Soc. 139 (7), 2657–2663. https://doi.org/10.1021/jacs.6b10841.

Corinaldesi, V., Mazzoli, A., Siddique, R., 2016. Characterization of lightweight mortars containing wood processing by-products waste. Constr. Build. Mater. 123, 281–289. https://doi.org/10.1016/j.conbuildmat.2016.07.011.

Deng, H., Skipa, T., Bilotti, E., Zhang, R., Lellinger, D., Mezzo, L., Fu, Q., Alig, I., Peijs, T., 2010. Preparation of high-performance conductive polymer fibers through morphological control of networks formed by nanofillers. Adv. Funct. Mater. 20 (9), 1424–1432. https://doi.org/10.1002/adfm.200902207.

Fawcett, W., Shetty, D.K., 2010. Effects of carbon nanofibers on cell morphology, thermal conductivity and crush strength of carbon foam. Carbon 48 (1), 68–80. https://doi.org/10.1016/j.carbon.2009.08.032.

Fayos, J., 1999. Possible 3D carbon structures as progressive intermediates in graphite to diamond phase transition. J. Solid State Chem. 148 (2), 278–285. https://doi.org/10.1006/jssc.1999.8448.

Gallego, N., Klett, J., 2003. Carbon Foams For Thermal Management. Carbon 41, 1461–1466. https://doi.org/10.1016/S0008-6223(03)00091-5.

Girgis, B.S., Yunis, S.S., Soliman, A.M., 2002. Characteristics of activated carbon from peanut hulls in relation to conditions of preparation. Mater. Lett. 57 (1), 164–172. https://doi.org/10.1016/S0167-577X(02)00724-3.

Gonçalves, A.A., Costa, M.J., Zhang, L., Ciesielczyk, F., Jaroniec, M., 2018. One-pot synthesis of $MeAl_2O_4$ (Me= Ni, Co, or Cu) supported on γ-Al_2O_3 with ultralarge mesopores: enhancing interfacial defects in γ-Al_2O_3 to facilitate the formation of spinel structures at lower temperatures. Chem. Mat. 30 (2), 436–446. https://doi.org/10.1021/acs.chemmater.7b04353.

He, X., Zhang, N., Shao, X., Wu, M., Yu, M., Qiu, J., 2016. A layered-template-nanospace-confinement strategy for production of corrugated graphene nanosheets from petroleum pitch for supercapacitors. Chem. Eng. J. 297, 121–127. https://doi.org/10.1016/j.cej.2016.03.153.

Hull, A., 1926. Ber. Dtsch. Chem. Ges. 59, 2433-2444.

Imai, A., Hardi, F., Lundqvist, P., Furusjö, E., Kirtania, K., Karagöz, S., Tekin, K., Yoshikawa, K., 2018. Alkali-catalyzed hydrothermal treatment of sawdust for production of a potential feedstock for catalytic gasification. Appl. Energy 231, 594–599. https://doi.org/10.1016/j.apenergy.2018.09.150.

Inagaki, M., Qiu, J., Guo, Q., 2015. Carbon Foam: Preparation and Application. Carbon 87, 128–152. https://doi.org/10.1016/j.carbon.2015.02.021.

Jana, P., Fierro, V., Pizzi, A., Celzard, A., 2014. Biomass-Derived, Thermally Conducting, Carbon Foams For Seasonal Thermal Storage. Biomass-.-. Bioenergy 67, 312–318. https://doi.org/10.1016/j.biombioe.2014.04.031.

Kang, E., Jung, Y.S., Cavanagh, A.S., Kim, G.H., George, S.M., Dillon, A.C., Kim, J.K., Lee, J., 2011. Fe_3O_4 nanoparticles confined in mesocellular carbon foam for high performance anode materials for lithium-ion batteries. Adv. Funct. Mater. 21 (13), 2430–2438. https://doi.org/10.1002/adfm.201002576.

Kang, D., Lee, J.W., 2016. Enhanced methane decomposition over nickel–carbon–B_2O_3 core–shell catalysts derived from carbon dioxide. Appl. Catal. B: Environ. 186, 41–55. https://doi.org/10.1016/j.apcatb.2015.12.045.

Kılıç, E., 2019. Preparation and Characterization of Graphene-Based Green Nanocomposites and Their Utilization in Various Applications. Doctor of Philosophy, Department of Chemistry, Hacettepe University, Ankara, Turkey.

Lei, S., Guo, Q., Liu, L., 2010. Preparation of Phenolic-Based Carbon Foam With Controllable Pore Structure and High Compressive Strength. Carbon 15 (03), 2644–2646. https://doi.org/10.1016/j.carbon.2010.03.017.

Li, W., Huang, Z., Wu, Y., Zhao, X., Liu, S., 2015. Honeycomb carbon foams with tunable pore structures prepared from liquefied larch sawdust by self-foaming. Ind. Crops Prod. 64, 215–223. https://doi.org/10.1016/j.indcrop.2014.09.043.

Li, D., Li, Y., Liu, H., Ma, J., Liu, Z., Gai, C., Jiao, W., 2019. Synthesis of biomass tar-derived foams through spontaneous foaming for ultra-efficient herbicide removal from aqueous solution. Sci. Total Environ. 673, 110–119. https://doi.org/10.1016/j.scitotenv.2019.04.057.

Li, S., Tian, Y., Zhong, Y., Yan, X., Song, Y., Guo, Q., Shi, J., Liu, L., 2011. Formation mechanism of carbon foams derived from mesophase pitch. Carbon 49 (2), 618–624. https://doi.org/10.1016/j.carbon.2010.10.007.

Li, J., Wang, C., Zhan, L., Qiao, W.M., Liang, X.Y., Ling, L.C., 2009. Carbon foams prepared by supercritical foaming method. Carbon 47 (4), 1204–1206. https://doi.org/10.1016/j.carbon.2009.01.015.

Lipson, H., Stokes, A.R., 1942. A new structure of carbon, 328-328 Nature 149 (3777). https://doi.org/10.1038/149328a0.

Lopez, F.A., Centeno, T.A., Garcia-Diaz, I., Alguacil, F.J., 2013. Textural and fuel characteristics of the chars produced by the pyrolysis of waste wood, and the properties of activated carbons prepared from them. J. Anal. Appl. Pyrol. 104, 551–558. https://doi.org/10.1016/j.jaap.2013.05.014.

Luo, X., Mohanty, A., Misra, M., 2013. Lignin as a reactive reinforcing filler for water-blown rigid biofoam composites from soy oil-based polyurethane. Ind. Crops Prod. 47, 13–19. https://doi.org/10.1016/j.indcrop.2013.01.040.

Mercuri, R.A., Wessendorf, T.R., Criscione, J.M., 1968. Carbon foam: its preparation and properties. Prepr. - Am. Chem. Soc., Div. Pet. Chem. 12 (4).

Mochida, I., Korai, Y., Ku, C.H., Watanabe, F., Sakai, Y., 2000. Chemistry of synthesis, structure, preparation and application of aromatic-derived mesophase pitch. Carbon 38 (2), 305–328. https://doi.org/10.1016/S0008-6223(99)00176-1.

Nicholson, J., Thomas, C., 1973. Syntactic Carbon Foams. Carbon 65–66. https://doi.org/10.1016/0008-6223(73)90009-2.

Ning, F., Cong, W., Hu, Y., Wang, H., 2017. Additive manufacturing of carbon fiber-reinforced plastic composites using fused deposition modeling: Effects of process parameters on tensile properties. J. Compos. Mater. 51 (4), 451–462. https://doi.org/10.1177/0021998316646169.

Ozbay, N., Yargic, A.S., 2019. Carbon foam production from bio-based polyols of liquefied spruce tree sawdust: Effects of biomass/solvent mass ratio and pyrolytic oil addition. J. Appl. Polym. Sci. 136 (11), 47185. https://doi.org/10.1002/app.47185.

Peng, H., Yao, B., Wei, X., Liu, T., Kou, T., Xiao, P., Zhang, Y., Li, Y., 2019. Pore and heteroatom engineered carbon foams for supercapacitors. Adv. Energy Mater. 9 (19), 1803665. https://doi.org/10.1002/aenm.201803665.

Pham, L., Truong, M.D., Nguyen, T.H., Le, L., Nam, N.D., Bach, L.G., Nguyen, V.T., Tran, N.Q., 2019. A dual synergistic of curcumin and gelatin on thermal-responsive hydrogel based on Chitosan-P123 in wound healing application. Biomed. Pharmacother. 117, 109183. https://doi.org/10.1016/j.biopha.2019.109183.

Prauchner, M.J., Pasa, V.M., de Menezes, S.M., 2001b. Solid-state ^{13}C NMR quantitative study of Eucalyptus tar pitches. J. Wood Chem. Technol. 21 (4), 371–385. https://doi.org/10.1081/WCT-100108332.

Prauchner, M.J., Pasa, V.M., Molhallem, N.D., Otani, C., Otani, S., Pardini, L.C., 2005. Structural evolution of Eucalyptus tar pitch-based carbons during carbonization. Biomass-.-. Bioenergy 28 (1), 53–61. https://doi.org/10.1016/j.biombioe.2004.05.004.

Prauchner, M.J., Pasa, V.M., Otani, C., Otani, S., 2001a. Characterization and thermal polymerization of Eucalyptus tar pitches. Energ. Fuels 15 (2), 449–454. https://doi.org/10.1021/ef000196o.

Sihn, S., Ganguli, S., Anderson, D.P., Roy, A.K., 2012. Enhancement of through-thickness thermal conductivity of sandwich construction using carbon foam. Compos. Sci. Technol. 72 (7), 767–773. https://doi.org/10.1016/j.compscitech.2012.02.003.

Strano, M.S., Zydney, A.L., Barth, H., Wooler, G., Agarwal, H., Foley, H.C., 2002. Ultrafiltration membrane synthesis by nanoscale templating of porous carbon. J. Membr. Sci. 198 (2), 173–186. https://doi.org/10.1016/S0376-7388(01)00574-9.

Sun, Y., Webley, P.A., 2011. Preparation of activated carbons with large specific surface areas from biomass corncob and their adsorption equilibrium for methane, carbon dioxide, nitrogen, and hydrogen. Ind. Eng. Chem. Res. 50 (15), 9286–9294. https://doi.org/10.1021/ie1024003.

Tondi, G., Pizzi, A., Delmotte, L., Parmentier, J., Gadiou, R., 2010. Chemical activation of tannin–furanic carbon foams. Ind. Crops Prod. 31 (2), 327–334. https://doi.org/10.1016/j.indcrop.2009.11.013.

Tsyntsarski, B., Petrova, B., Budinova, T., Petrov, N., Krzesinska, M., Pusz, S., Majewska, J., Tzvetkov, P., 2010. Carbon foam derived from pitches modified with mineral acids by a low pressure foaming process. Carbon 48 (12), 3523–3530. https://doi.org/10.1016/j.carbon.2010.05.048.

Tushar, M.S.H.K., Mahinpey, N., Khan, A., Ibrahim, H., Kumar, P., Idem, R., 2012. Production, characterization and reactivity studies of chars produced by the isothermal pyrolysis of flax straw. Biomass-.-. Bioenergy 37, 97–105. https://doi.org/10.1016/j.biombioe.2011.12.027.

Wang, J., Kaskel, S., 2012. KOH activation of carbon-based materials for energy storage. J. Mater. Chem. 22 (45), 23710–23725. https://doi.org/10.1039/C2JM34066F.

Wang, M.X., Wang, C.Y., Li, T.Q., Hu, Z.J., 2008. Preparation of mesophase-pitch-based carbon foams at low pressures. Carbon 46 (1), 84–91. https://doi.org/10.1016/j.carbon.2007.10.038.

Wang, C., Yan, B., Zheng, J., Feng, L., Chen, Z., Zhang, Q., Liao, T., Chen, J., Jiang, S., Du, C., He, S., 2022. Recent progress in template-assisted synthesis of porous carbons for supercapacitors. Adv. Powder Mater. 1 (2), 100018. https://doi.org/10.1016/j.apmate.2021.11.005.

Wang, G., Zhao, J., Wang, G., Zhao, H., Lin, J., Zhao, G., Park, C.B., 2020. Strong and super thermally insulating in-situ nanofibrillar PLA/PET composite foam fabricated by high-pressure microcellular injection molding. Chem. Eng. J. 390, 124520. https://doi.org/10.1016/j.cej.2020.124520.

Wu, J., Li, H., Lai, X., Chen, Z., Zeng, X., 2020. Conductive and superhydrophobic F-rGO@CNTs/chitosan aerogel for piezoresistive pressure sensor. Chem. Eng. J. 386, 123998. https://doi.org/10.1016/j.cej.2019.123998.

Xiong, S., Fan, J., Wang, Y., Zhu, J., Yu, J., Hu, Z., 2017. A facile template approach to nitrogen-doped hierarchical porous carbon nanospheres from polydopamine for high-performance supercapacitors. J. Mater. Chem. A 5 (34), 18242–18252. https://doi.org/10.1039/C7TA05880B.

Xiong, W., Liu, M., Gan, L., Lv, Y., Xu, Z., Hao, Z., Chen, L., 2012. Preparation of nitrogen-doped macro-/mesoporous carbon foams as electrode material for supercapacitors. Colloids Surf. A: Physicochem. Eng. Asp. 411, 34–39. https://doi.org/10.1016/j.colsurfa.2012.06.042.

Xu, X., Guan, C., Xu, L., Tan, Y.H., Zhang, D., Wang, Y., Zhang, H., Blackwood, D.J., Wang, J., Li, M., Ding, J., 2019. Three dimensionally free-formable graphene foam with designed structures for energy and environmental applications. ACS Nano 14 (1), 937–947. https://doi.org/10.1021/acsnano.9b08191.

Yargic, A.S., 2021. Current Engineering Sciences Research, Chapter-1-Conversion of Biopitch to Carbon Foam with Tunable Properties: The Role of Chemical Activation, Livre de Lyon, Lyon,1-22.

Yargic, A.S., Gunduz Meric, G., Yarbay, R.Z., Ozbay, N., 2023. Investigation of CO_2 sequestration performance and statistical analysis of dye removal efficiency of liquefied hornbeam based carbon foams: Effects of biomass/solvent weight ratio, tar contribution, and chemical activation. Mater. Today Sustain. 24, 100517. https://doi.org/10.1016/j.mtsust.2023.100517.

Yargic, A.S., Ozbay, N., 2019. Effect of chemical activation on the cellular structure of biopitch-derived green carbon foam. Diam. Relat. Mater. 96, 58–66. https://doi.org/10.1016/j.diamond.2019.04.032.

Yargıç, A.Ş., 2017. Production and characterization of carbon foam. Doctor of Philosophy, Department of Chemical Engineering, Bilecik Seyh Edebali University and Anadolu University Joint Postgraduate Education Program, Bilecik, Turkey.

Yargıç, A.Ş., Gündüz Meriç, G., Dolaş, Y., Özbay, N., 2021b. Production and Characterization of Open-Celled Carbon Foams from Sawmill Waste. Bilecik Seyh Edebali Univ. J. Sci. 8 (2), 1044–1056. https://doi.org/10.35193/bseufbd.1013724.

Yargıç, A.Ş., Şahin, R.Z.Y., Özbay, N., 2021a. Investigation of solvent type effect on the structural properties of bio-polyol-based carbon foam. J. Fac. Eng. Archit. Gazi Univ. 36 (1), 133–145. https://doi.org/10.17341/gazimmfd.673657.

Yousefi, N., Sun, X., Lin, X., Shen, X., Jia, J., Zhang, B., Tang, B., Chan, M., Kim, J.K., 2014. Highly aligned graphene/polymer nanocomposites with excellent dielectric properties for high-performance electromagnetic interference shielding. Adv. Mater. 26 (31), 5480–5487. https://doi.org/10.1002/adma.201305293.

Zakaria, M.B., Suzuki, N., Torad, N.L., Matsuura, M., Maekawa, K., Tanabe, H., Yamauchi, Y., 2013. Preparation of mesoporous titania thin films with well-crystallized frameworks by using thermally stable triblock copolymers. Eur. J. Inorg. Chem. 2013 (13), 2330–2335. https://doi.org/10.1002/ejic.201201305.

Zhang, Y., Qiu, M., Yu, Y., Wen, B., Cheng, L., 2017. A novel polyaniline-coated bagasse fiber composite with core–shell heterostructure provides effective electromagnetic shielding performance. ACS Appl. Mater. Interfaces 9 (1), 809–818. https://doi.org/10.1021/acsami.6b11989.

Zhang, S., Zheng, M., Lin, Z., Li, N., Liu, Y., Zhao, B., Pang, H., Cao, J., He, P., Shi, Y., 2014. Activated carbon with ultrahigh specific surface area synthesized from natural plant material for lithium–sulfur batteries. J. Mater. Chem. A 2 (38), 15889–15896. https://doi.org/10.1039/C4TA03503H.

Zhang, H., Zhou, Y., Li, C., Chen, S., Liu, L., Liu, S., Yao, H., Hou, H., 2015. Porous nitrogen doped carbon foam with excellent resilience for self-supported oxygen reduction catalyst. Carbon 95, 388–395. https://doi.org/10.1016/j.carbon.2015.08.025.

Zhao, Q., Wang, X., Liu, J., Wang, H., Zhang, Y., Gao, J., Lu, Q., Zhou, H., 2015. Design and synthesis of three-dimensional hierarchical ordered porous carbons for supercapacitors. Electrochim. Acta 154, 110–118. https://doi.org/10.1016/j.electacta.2014.12.052.

Zou, S., Li, H., Wang, S., Jiang, R., Zou, J., Zhang, X., Liu, L., Zhang, G., 2020. Experimental research on an innovative sawdust biomass-based insulation material for buildings. J. Clean. Prod. 260, 121029. https://doi.org/10.1016/j.jclepro.2020.121029.